




BRIEF COMMUNICATION

Activation of LiCoPO₄ in Air

ABDELAZIZ M. ABORAIA ^{1,2,6} V.V. SHAPOVALOV,¹ A.A. GUDA,¹
V.V. BUTOVA,^{1,3} H.Y. ZAHRAN,^{4,5} I.S. YAHIA,^{4,5} and A.V. SOLDATOV¹

1.—The Smart Materials Research Institute, Southern Federal University, Sladkova 178/24, Rostov-on-Don, Russia 344090. 2.—Department of Physics, Faculty of Science, Al-Azhar University, Assiut 71542, Egypt. 3.—Federal Research Center of the Southern Scientific Center of the Russian Academy of Sciences, Rostov-on-Don, Russia 344006. 4.—Advanced Functional Materials and Optoelectronic Laboratory (AFMOL), Department of Physics, Faculty of Science, King Khalid University, P. O. Box 9004, Abha, Saudi Arabia. 5.—Metallurgical Lab., Nanoscience Laboratory for Environmental and Bio-medical Applications (NLEBA), Semiconductor Lab., Physics Department, Faculty of Education, Ain Shams University, Roxy, Cairo 11757, Egypt. 6.—e-mail: a.m.aboraia@gmail.com

LiCoPO₄ was synthesized in a short time by a microwave-assisted solvothermal technique at 220°C. The as-prepared samples are characterized as belonging to the *Pn21a* symmetry group, having poor electrochemical performance, and low specific capacity around 30 mAh/g. Further, activation at 700°C under air and argon increased the specific capacity to 57 mAh/g and 55 mAh/g, respectively. The local atomic and electronic structure of the samples before and after annealing was studied using x-ray absorption spectroscopy (XAS). The activation under air and Ar led to a phase transition from the *Pn21a* space group to the *Pnma* space group without changes in the Co oxidation state. Therefore, using myristic acid as a source for carbon coating, we found that there were no specific requirements for the activation atmosphere.

Key words: Li-ion batteries, LiCoPO₄, XANES, phase transition, electrochemistry, oxidation state

INTRODUCTION

Recent studies favor the practical use of LiMPO₄ (M = Fe, Co, Ni, and Mn) olivines as effective and low-cost cathode materials. For instance, LiFePO₄, first among this class of cathodes, has already found its application in commercial Li-ion cells, demonstrating good electrochemical performance, a working potential of 3.4V (versus Li/Li+), and a specific energy around 578 Wh/kg. However, most olivines critically lack electroconductivity (less than 10⁻⁹ S/cm), which can be only partially improved by using nanosized particles and activating the surface conductivity with increased carbon content in a cathode composite.^{1,2} Many applications also require a cell potential higher than one available with Fe-

olivines, so novel research work is focused on LiCoPO₄, which has a high potential (around 5 V versus Li/Li+), a high theoretical capacity of 167 mAh/g, and an increased theoretical gravimetric energy density of up to 800Wh/kg with low cost.³⁻⁶ However, the high voltage, which is a feature of this material, requires the use of modified electrolytes, since standard electrolytes (like 1M LiPF₆ in 1:1 EC: DMC) are not stable at such potentials. Moreover, LiCoPO₄ has poor electrochemical performance and a limited life cycle (around 500-1000 cycles). These issues are addressed by reducing particle size, doping by transition metals (Fe, Mn, and Ni), and modifying the surface by coating it with carbon to enhance its conductivity.⁷⁻¹⁰

There are several methods available to synthesize LiCoPO₄. One is a solid-state method that takes roughly one day to obtain a material with a specific capacity in a range of 31 mAh/g to 128 mAh/g (1st

(Received October 3, 2020; accepted March 6, 2021)

discharge) and particle sizes in a range between 50 nm and 10 μm .^{11–13} Another technique is hydrothermal synthesis, which is suitable for the preparation of nanosized LiCoPO_4 , but is also time-consuming and provides specific capacity of 52 mAh/g to 137 mAh/g (first discharge).^{14,15} A sol-gel approach can be used to obtain highly homogeneous nanosized materials at a low cost. However, this requires the longest time to process, and the capacity of the resulting material ranges from 63 mAh/g to 137 mAh/g (1st discharge). Microwave radiation can significantly reduce the time required for nanocrystal formation.¹⁶ In the present work, we use low-temperature microwave (MW)-assisted solvothermal synthesis, which requires only 3 hours to obtain LiCoPO_4 with a specific capacity in a range of 52 mAh/g to 141 mAh/g (1st discharge).^{15,17}

Olivine LiCoPO_4 has three polymorphic forms: *Pn21a*, *Pnma*, and *Cmcm*.^{5,14} The *Pn21a* space group of LiCoPO_4 can be synthesized by a MW-assisted solvothermal method at 220°C with ethylene glycol. It is a metastable phase with poor electrochemical performance and a low specific capacity equal to 7–30 mAh/g, which may be attributed to the fact that the surface of the material is not appropriately activated due to the low synthesis temperature.¹⁸ Formation of structures in the *Cmcm* space group was reported by two different methods: high pressure/temperature solid-state methods (6 GPa/900°C)^{15,17} and by MW-assisted solvothermal synthesis at 260°C and a pressure lower than 30 bar.¹⁹ The transformation from *Pn21a* to *Pnma* phases requires a temperature higher than 500°C.¹⁹ Usually, this activation is performed under argon at 700°C, and the resulting material has better electrochemical performance and specific capacity, typically from 50 mAh/g to 132 mAh/g.^{15,17,18,20} However, the first attempts to use atmospheres other than Ar resulted in the presence of secondary phases or poor specific capacities.²¹

Kotobuki et al. recently proposed a one-step coating process using carboxymethylcellulose as a precursor during the hydrothermal synthesis of LiCoPO_4 with different sources of Co, which affected the resulting specific capacity.²² We use a similar approach and propose adding a long-chain acid (myristic acid) as a source of carbon during synthesis to dramatically improve the adhesion of the conductive coating to particles of the material. Resulting samples were activated both under the inert atmosphere and in air and compared using element-selective Co K-edge x-ray absorption spectroscopy (XAS), x-ray diffraction (XRD), and electrochemical cycling.

METHODS

Two solutions, A and B, were used for the synthesis. Solution A: 0.0735g of $\text{LiOH}\cdot\text{H}_2\text{O}$ was dissolved in 333 μL of water, and 6.67 mL of

ethylene glycol was added. Solution B: 0.0420g of $\text{LiOH}\cdot\text{H}_2\text{O}$ was dissolved in 1 ml water, 68.3 μL of H_3PO_4 was added. After this, the volume of solution B was adjusted to 3 ml with water, and $\text{Co}(\text{NO}_3)_2\cdot 6\text{H}_2\text{O}$ (0.2910 g), $\text{C}_6\text{H}_{12}\text{O}_6$ (0.1026 g), and 1.5 g of myristic acid were added and mixed with a magnetic stirrer to obtain a homogeneous blue solution. Finally, solution A was added to solution B. The resulting mixture was placed in a Teflon vessel at 220°C for 3 h under 800 W power in a MW oven. The final blue precipitate was collected by centrifugation and was washed with ethanol and water three times. Then we split the product into two parts. One part was activated in an argon flow and the second part was activated in air for 5 hours at 700°C.²³

The XRD patterns of the resulting powder were recorded by a D2 Phaser laboratory x-ray diffractometer (Bruker, Germany) using $\text{Cu-K}\alpha_1$ radiation ($\lambda = 1.540598 \text{ \AA}$). Subsequent crystallographic structure refinement by the Rietveld technique was carried out using the FullProf Suite.²⁴ Cobalt K-edge XAS spectra of LiCoPO_4 samples were measured with an R-XAS Looper (Rigaku, Japan) laboratory spectrometer.

X-ray absorption spectra were measured in transmission geometry with a crystal Ge(311) as a monochromator, providing energy resolution $\Delta E = 1.9 \text{ eV}$ at the Co K-edge. The incident beam intensity was monitored by an Ar-filled (300 mbar) ionization chamber, with transmitted intensity measured by a scintillation counter with a photomultiplier tube. The samples for measurement were mixed with 50 mg of dry cellulose powder and pressed into pellets. The optimal mass for the sample powder was calculated using XAFSmass software.²⁵ Spectra for reference compounds (CoO , Co_3O_4) were measured in the same way to determine the charge state of Co in LiCoPO_4 via the chemical shift of the absorption edge.

The electrochemical performance of as-prepared and annealed materials was tested by galvanostatic charge/discharge using a P-20X potentiostat/galvanostat device (Elins, Russia). The materials were mortared with carbon black (Super P conductive) by weight in a ratio of 80%:20% active material to carbon. The resulting mixture was then placed into the cell as a cathode (7.5 mg/cm^2 load of active material) with Li foil as an anode. A glass microfiber filter (Whatman, grade GF/C) was used as a separator, and 1M LiPF_6 in EC/DMC = 50/50 (v/v) (Sigma Aldrich) as an electrolyte. The cells were assembled in an Ar-filled glove bag and cycled from 3 V to 5.1 V with a current of C/10 (where C is the theoretical cell capacity). To measure the electronic and ionic impedance resistance, the powder was pressed under 3 tons to form pellets with a thickness of 15 mm and a diameter of 10 mm. These pellets were sintered at 650°C for 2 h under air and cooled down slowly to room temperature. Both sides were then coated by graphene and acted as two

electrodes. An impedance in a frequency range of 1 MHz to 100 MHz with an AC amplitude of 10 mV was measured utilizing the PARSTAT 4000 potentiostat/galvanostat at room temperature. To prove the difference in the local structure, we calculated the theoretical spectra of different phases of LiCoPO_4 using the finite difference method implemented in FDMNES software.²⁶ The calculations were performed for atomic clusters of 6 Å around the absorbing atom (Co) and 0.2 Å grid interpoint distance.

RESULTS AND DISCUSSION

LiCoPO_4 was prepared by the MW-assisted solvothermal technique at a temperature of 220°C for 3 hours. Analysis of XRD patterns for the as-prepared sample proved that it contains an orthorhombic phase in the $Pn21a$ space group. The Rietveld refinement confirmed no phase impurities, since all peaks match tetrahedral coordinated LiCoPO_4 , as shown in Fig. 1a.

The phase with the $Pn21a$ space group is rarely studied since it has poor electrochemistry, which may be attributed to surface passivation.¹⁸ These properties can be improved upon activation. We show in Fig. 1b and c the resulting XRD patterns after activation in both air and an Ar atmosphere at 700°C. Annealed samples are characterized by the

$Pnma$ space group. Table I lists crystal lattice parameters obtained after XRD pattern refinement, and Table II shows atomic positions in the unit cell.

The surface of the obtained particles is activated upon annealing at high temperature. This process is expensive because it is usually performed under an argon atmosphere to avoid changing the oxidation state of Co or losing lithium at high temperatures. Using air as the activation atmosphere can significantly reduce the cost of this process for industrial applications. XRD analysis reveals no significant differences between the samples annealed in Ar or air, except a small increase in the lattice parameters by ca. 0.01 Å for the air-annealed sample. To address the local atomic and electronic structure around Co ions, we further performed measurements on the Co K-edge XANES spectra.

The experimental XANES spectra for two LiCoPO_4 samples before and after annealing under argon (Fig. 2) show dramatic differences indicating structural changes of the first coordination sphere around Co upon phase transition. In particular, the spectrum of the non-annealed sample has a clear pre-edge feature (~ 7710 eV) attributed to the electronic transition from the 1s state to the 3d states hybridized with the Co 4p states in tetrahedral symmetry. The intensity of the pre-edge peak for

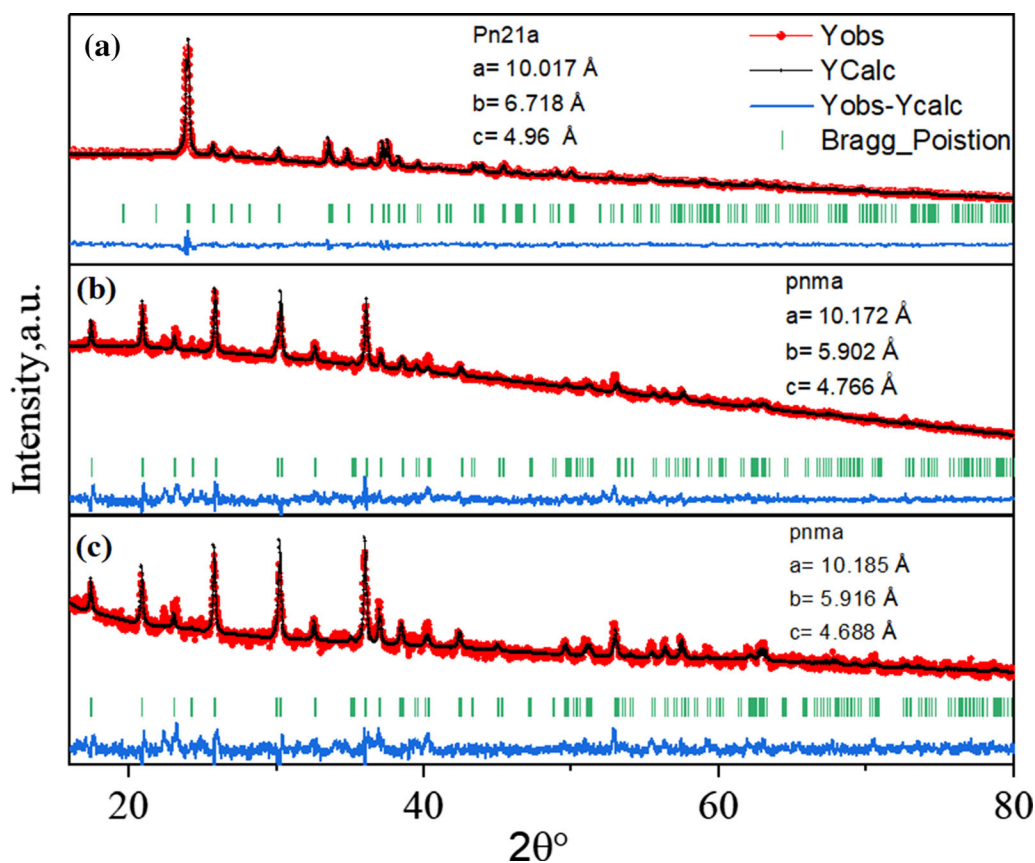


Fig. 1. Rietveld refinement of experimental XRD patterns for LiCoPO_4 (a) tetrahedral phase with $Pn21a$ space group before annealing, (b) olivine phase with $Pnma$ space group after annealing under argon, (c) olivine phase with $Pnma$ space group after annealing under air.

Table I. Lattice parameters for LiCoPO₄ as synthesized, after annealing in air, and after annealing under Ar

Composition	Conditions	Space group	<i>a</i> (Å)	<i>b</i> (Å)	<i>c</i> (Å)	Unit cell volume (Å ³)
LiCoPO ₄	As synthesized	<i>Pn21a</i>	10.017	6.718	4.960	333.795
LiCoPO ₄	Annealing 700°C, Ar	<i>Pnma</i>	10.172	5.902	4.676	280.755
LiCoPO ₄	Annealing 700°C, air	<i>Pnma</i>	10.185	5.916	4.688	282.465

Table II. Refined atomic positions for the unit cell of synthesized LiCoPO₄ with different space groups and annealing atmospheres

Atoms	X	Y	Z
LiCoPO ₄ , <i>Pn21a</i> space group (before activation)			
Li	0.867	0.970	0.334
Co	0.342	0.399	0.192
P	0.412	0.665	0.676
O	0.352	0.478	0.827
O	0.142	0.321	0.306
O	0.393	0.662	0.354
O	0.451	0.183	0.218
LiCoPO ₄ , <i>Pnma</i> space group (activation under Ar)			
Co	0.724	0.250	0.522
P	0.591	0.750	0.573
O	0.686	0.512	0.672
O	0.450	0.750	0.724
O	0.606	0.750	0.245
Li	0.500	0.500	1.000
LiCoPO ₄ , <i>Pnma</i> space group (activation under air)			
Co	0.725	0.250	0.501
P	0.601	0.750	0.562
O	0.673	0.468	0.755
O	0.454	0.750	0.704
O	0.590	0.750	0.262
Li	0.500	0.500	1.000

the annealed sample becomes smaller and therefore suggests distorted octahedral coordination of Co.

The position of the absorption edge (~ 7710 eV) in the XANES spectra of LiCoPO₄ in the *Pn21a* and *Pnma* space groups is close to that in CoO, which means that they both contain divalent cobalt ions. Despite the similar oxidation states of Co in LiCoPO₄ before and after annealing, the local atomic structure undergoes significant transformation upon phase transition. We have simulated the XANES spectra for crystallographic structures of LiCoPO₄ in the *Pn21a* and *Pnma* space groups (COD entry #2300246) and (ICSD entry #187759). Figure 2 shows that there is good agreement between changes in the experimental spectra compared to the simulated ones. Therefore, we can confirm that the initially tetrahedral coordination of Co reorganized to octahedral coordination in the *Pnma* phase.

In Fig. 3 we compare two experimental spectra for samples after annealing in air and argon. Both samples are characterized by the same Co²⁺ oxidation state and correspond to the theoretical XANES spectrum for the olivine phase.

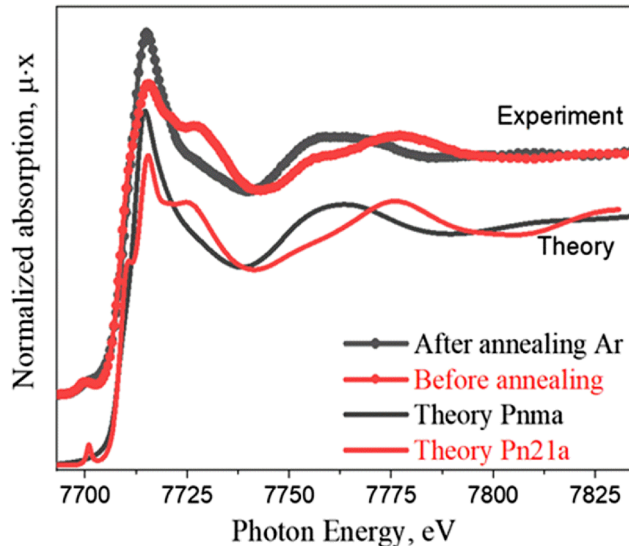


Fig. 2. Comparison between experimental Co K-edge XANES spectra for LiCoPO₄ as synthesized and annealed under Ar (upper curves) along with theoretical calculations for LiCoPO₄ with *Pn21a* and *Pnma* space groups (bottom curves). The smaller energy resolution of the theoretical spectra relative to the experimental energy resolution was chosen to highlight the differences in the pre-edge and main edge intensities.

The samples were further characterized by galvanostatic charge and discharge (Fig. 4). The discharge capacities measured for powder before annealing, after annealing under argon, and after annealing in air in the 1st cycle were 30 mAh/g, 55 mAh/g, and 57 mAh/g, respectively. The specific capacity of the *Pn21a* phase is close to the previously reported data.^{14,18} LiCoPO₄ particles covered by the long-chain acid introduced sufficient carbon coating upon annealing. Figure S1 in SI shows the enhanced electronic conductivity of the material measured with impedance spectroscopy. First-discharge specific capacity for the air-annealed *Pnma*-LiCoPO₄ phase is similar to the Ar-annealed sample and agrees with the data reported for the carbon-coated LiCoPO₄ compounds.^{11,27} Furthermore, we note that the capacity fade for both materials is very similar in the first several cycles, which makes both Ar and air atmospheres identical in terms of cycling performance, as demonstrated in Fig. S2. Optimization of the material performance can be achieved by tuning the synthesis procedure to avoid mixed-ion

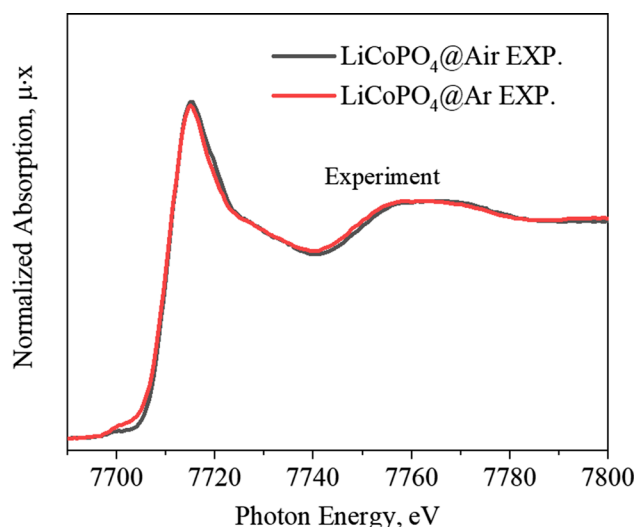


Fig. 3. Experimental Co K-XANES spectra for LiCoPO₄ after annealing under argon and air.

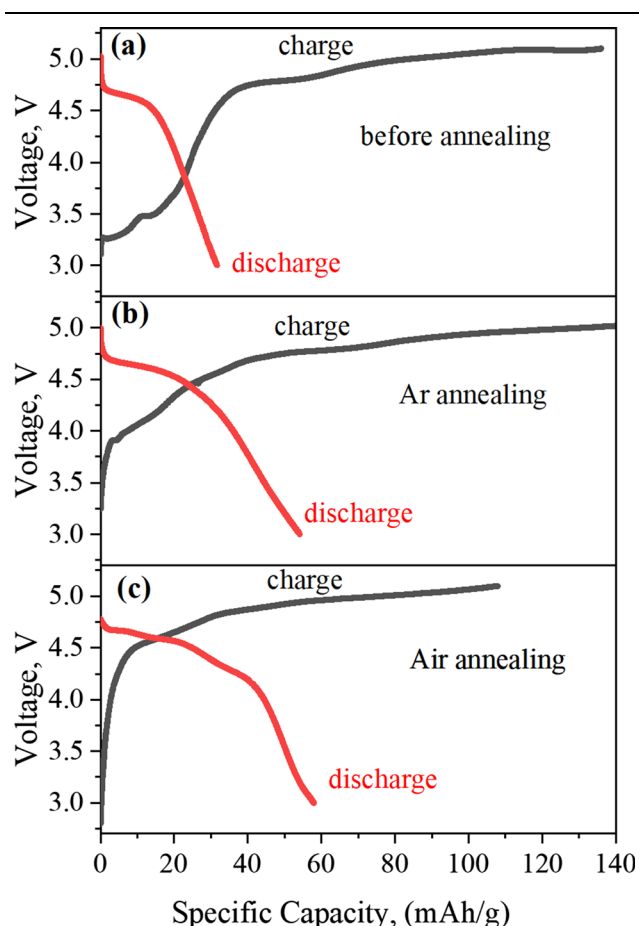


Fig. 4. First cycle of galvanostatic charge-discharge for (a) LiCoPO₄ before annealing (space group *Pn21a*). (b) LiCoPO₄ after annealing under argon (space group *Pnma*). (c) LiCoPO₄ after annealing in air (space group *Pnma*).

occupation and anti-site defects where Co blocks Li diffusion, or by increasing the high-voltage stability of the electrolyte by adding decomposition-inhibiting additives.¹⁸

CONCLUSION

LiCoPO₄ powder samples were prepared by a MW-assisted solvothermal technique at a low temperature. XRD proved that the as-synthesized material has orthorhombic symmetry within the *Pn21a* space group. To enhance electrochemical performance, we inserted long-chain myristic acid as a source of carbon during the preparation. The samples were activated under two different atmospheres, argon and air, at 700°C. The Co K-XAS spectra revealed no prominent changes for samples in the oxidizing atmosphere as compared to the inert one. Therefore, the cobalt oxidation state and local atomic structure in the sample annealed in the air atmosphere was similar to the one obtained upon Ar annealing. Using air for the activation of coated LiCoPO₄ provides a way to lower the costs of industrial applications. As-synthesized LiCoPO₄ with the *Pn21a* space group has a poor discharge capacity of only 30 mAh/g in the first cycle. After activation and transition to the *Pnma* space group, the discharge capacity increased to 55 mAh/g and 57 mAh/g for Ar- and air-activated samples. Our study shows that the oxidative air atmosphere can be used for activation of the myristic-acid-coated LiCoPO₄ without oxidation of the Co ions and without influencing the electrochemical performance of the material.

ACKNOWLEDGMENTS

The work was financially supported by the Ministry of Science and Higher Education of the Russian Federation (State assignment in the field of scientific activity, № 0852-2020-0019).

CONFLICT OF INTEREST

The authors of this article declare that they have no conflict of interest.

SUPPLEMENTARY INFORMATION

The online version contains supplementary material available at <https://doi.org/10.1007/s11664-021-08870-3>.

REFERENCES

1. O.A. Podgornova, and N.V. Kosova, *Chem. Sustain. Dev.* **22**, 53 (2014).
2. F.C. Strobridge, H. Liu, M. Leskes, O.J. Borkiewicz, K.M. Wiaderek, P.J. Chupas, K.W. Chapman, and C.P. Grey, *Chem. Mater.* **28**, 3676 (2016).
3. F. Zhou, M. Cococcioni, K. Kang, and G. Ceder, *Electrochem. Commun.* **6**, 1144 (2004).
4. J. Manzi, M. Curcio, and S. Brutti, *Nanomaterials* **5**, 2212 (2015).
5. K.J. Kreder Iii, G. Assat, and A. Manthiram, *Chem. Mater.* **27**, 5543 (2015).

6. Y.-M. Kang, Y.-I. Kim, M.-W. Oh, R.-Z. Yin, Y. Lee, D.-W. Han, H.-S. Kwon, J.H. Kim, and G. Ramanath, *Energy Environ. Sci.* 4, 4978 (2011).
7. L.Y. Xing, M. Hu, Q. Tang, J.P. Wei, X. Qin, and Z. Zhou, *Electrochim. Acta* 59, 172 (2012).
8. Q.D. Truong, M.K. Devaraju, Y. Ganbe, T. Tomai, and I. Honma, *Sci. Rep.* 4, 1 (2014).
9. D. Di Lecce, J. Manzi, F.M. Vitucci, A. De Bonis, S. Panero, and S. Brutti, *Electrochim. Acta* 185, 17 (2015).
10. S. Brutti, J. Manzi, D. Meggiolaro, F.M. Vitucci, F. Tre-quattrini, A. Paolone, and O. Palumbo, *J. Mater. Chem. A Mater.* 5, 14020 (2017).
11. L. Tan, Z. Luo, H. Liu, and Y. Yu, *J. Alloys Compd.* 502, 407 (2010).
12. J. Wolfenstine, and J. Allen, *J. Power Sour.* 136, 150 (2005).
13. I.-C. Jang, H.H. Lim, S.B. Lee, K. Karthikeyan, V. Aravindan, K.S. Kang, W.S. Yoon, W.I. Cho, and Y.S. Lee, *J. Alloys Compd.* 497, 321 (2010).
14. C. Jähne, C. Neef, C. Koo, H.-P. Meyer, and R. Klingeler, *J. Mater. Chem. A Mater.* 1, 2856 (2013).
15. M. Zhang, N. Garcia-Araez, and A.L. Hector, *J. Mater. Chem. A Mater.* 6, 14483 (2018).
16. Y.-J. Zhu, and F. Chen, *Chem. Rev.* 114, 6462 (2014).
17. J. Ludwig, C. Marino, D. Haering, C. Stinner, H.A. Gasteiger, and T. Nilges, *J. Power Sour.* 342, 214 (2017).
18. J. Ludwig, D. Nordlund, M.M. Doeff, and T. Nilges, *J. Solid State Chem.* 248, 9 (2017).
19. C. Alarcón-Suesca, J. Ludwig, V. Hlukhyy, C. Stinner, and T. Nilges, *Inorganics* 4, 35 (2016).
20. J. Ni, L. Gao, and L. Lu, *J. Power Sour.* 221, 35 (2013).
21. L. Dimesso, S. Jacke, C. Spanheimer, and W. Jaegermann, *J. Solid State Electrochem.* 16, 911 (2012).
22. M. Kotobuki, *Int. J. Energy Environ. Eng.* 4, 25 (2013).
23. A.M. Aboraia, V.V. Shapovalov, K. Vetlitsyna-Novikova, A.A. Guda, V.V. Butova, H.Y. Zahran, I.S. Yahia, and A.V. Soldatov, *J. Phys. Chem. Solids* 136, 109192 (2020).
24. C. Frontera and J. Rodríguez-Carvajal, *Physica B Condens Matter*, 335, 219 (2003).
25. K. Klementiev, R. Chernikov, XAFSmass: a program for calculating the optimal mass of XAFS samples, pp. 012008.
26. S.A. Guda, A.A. Guda, M.A. Soldatov, K.A. Lomachenko, A.L. Bugaev, C. Lamberti, W. Gawelda, C. Bressler, G. Smolentsev, and A.V. Soldatov, *J. Chem. Theory Comput.* 11, 4512 (2015).
27. J.L. Shui, Y. Yu, X.F. Yang, and C.H. Chen, *Electrochem. Commun.* 8, 1087 (2006).

Publisher's Note Springer Nature remains neutral with regard to jurisdictional claims in published maps and institutional affiliations.